GLOBAL ENGINEERS & TECHNOLOGISTS REVIEW
www.getview.org

INTEGRATING SPUR GEAR TEETH DESIGN AND ITS ANALYSIS WITH G² PARAMETRIC BÉZIER-LIKE CUBIC TRANSITION AND SPIRAL CURVES

YAHAYA[1], S.H., ALI[2], J.M., YAZARIAH[3], M.Y., HAERYIP SIHOMBING[4], and YUHAZRI[5], M.Y.

[1, 4, 5] Faculty of Manufacturing Engineering
Universiti Teknikal Malaysia Melaka
Hang Tuah Jaya, 76100 Durian Tunggal, Melaka, MALAYSIA
[1]saifudin@utem.edu.my
[4]iphaery@ utem.edu.my
[5]yuhazri@utem.edu.my

[2, 3] School of Mathematical Sciences
University of Science Malaysia
Minden, 11800, Penang, MALAYSIA
[2]jamaluma@cs.usm.my
[3]yazariahmy@cs.usm.my

ABSTRACT

An involute curve (or known as an approximated curve) is mostly used in designing the gear teeth (profile) especially in spur gear. Conversely, this study has the intention to redesign the spur gear teeth using the transition (S transition and C spiral) curves (also known as the exact curves) with curvature continuity (G²) as the degree of smoothness. Method of designing the transition curves is adapted from the circle to circle templates. The applicability of the new teeth model with the chosen material, Stainless Steel Grade 304 is determined using Linear Static Analysis, Fatigue Analysis and Design Efficiency (DE). Several concepts and the related examples are shown throughout this study.

Keywords: *Spur Gear Profile, S-Transition Curve, C-Spiral Curve, FEA, DE.*

1.0 INTRODUCTION

Gears are the most widely used elements in both applications such in consumer and industrial machineries. As we know, gear types may be grouped into five main categories, namely, spur, helical, rack and pinion, worm and bevel. As referred to in (Babu and Tsegaw, 2009; Bradford and Guillet, 1943; Higuchi and Gofuku, 2007), these are the most common curves used for the gear tooth profiles. These curves are developed based on the approximation theory, for instance; the development of involute curves has used a Chebyshev approximation (Higuchi and Gofuku, 2007). Besides, the tracing point method has also been applied along the path (shape) design of involute curves (Margalit, 1995; Reyes *et al.*, 2008; Yeung, 1999). Therefore, several methods and concepts have been employed in the generation of involute curves. With reference to the above evidence, it shows that this involute curve is not directly produced and is shown as the approximated (inexact) curves. For these reasons, we propose the theoretical developments of the exact (or known as the transition) curves using the parametric function.

Mathematically, parametric function is a method to define a relation between the independent (free) variables. Previously, Ali (1994) and Ali *et al.,* (1996) explored the parametric of Bézier-like cubic curve using Hermite interpolation. They are, however, only focused on the function developments, while the scope of designs through the proposed curves is not touched upon. Therefore, in this study, we use the Bézier-like cubic curve approach as the degree three (cubic) polynomial curves that allow the inflection points. This is due to the approach is suitable for G² (curvature) blending application curves and also contains the shape parameters which can control the shape of the curve (Ali, 1994; Ali *et al.*, 1996; Walton and Meek, 1999). As compared to the cubic Bézier curves, the shape parameters are not automatically included (Rashid and Habib, 2010; Habib and Sakai, 2008). Figure 1 shows the method of designing the transition curves will follow the five cases of clothoid templates as was identified by Baass (1984) and successfully used in highways or railways design. These templates are crucial to determine the design parameters in order to ensure the comfort and safety of road users (Baass, 1984). The templates are 1) straight line to circle, 2) circle to circle with C transition, 3) circle to circle with an S transition, 4) straight line to straight line and 5) circle to circle where one circle lies inside the other with a C transition (Walton and Meek, 1999; Baass, 1984; Walton and Meek, 1996). Figure 2 shows the profiles

design where the third and fifth templates are similar to the involute curves. In this study, these two templates with the application of Bézier-like cubic curve function are therefore chosen to redesign a spur gear teeth profile. By using the new method, the curve is directly generated with the significant increases in accuracy, and also the actual spur gear profile can be produced through this method.

This study will continue to find out the applicability of the new profile generation and the gear material through Stress-Strain Analysis, Fatigue Analysis and DE. FEA is the most common tools for the analysis while Stainless Steel Grade 304 is chosen for the selection of material in this study. This gear material is often selected for gear application since it has an aesthetic appearance, ease of fabrication and good in impact resistance. The scheme in Stress-Strain Analysis known as a Linear Static Analysis is used to determine many of the physical structures such in the stress, force and displacement distributions (Westland, 2006; Sapto and Safarudin, 2008). Many of the studies use this linear scheme to determine the structural applicability between the involute profiles and the gear material (Feng, 2011; Gurumani and Shanmugam, 2011; Reagor, 2010). However, there is no related study for the proposed curves. The retrieved values from Linear Static Analysis will be further explored in Fatigue Analysis and DE where both are strongly connected to the safety factor (Moultrie, 2009; Khai *et al*., 2007; Niederstucke *et al*., 2003; Firth and Long, 2010). Incidentally, the descriptions of DE in the design area are still less-decrypted. Figure 3 shows one of the applications using Linear Static Analysis. The next section will explain the nomenclature used in this study.

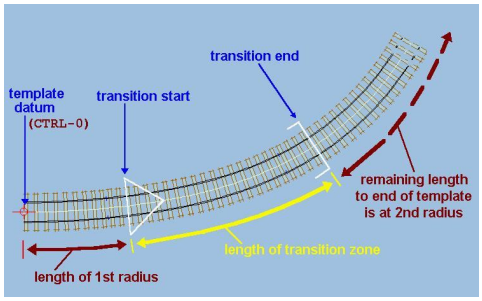

Figure 1: Railways route design modeling using transition curves application.

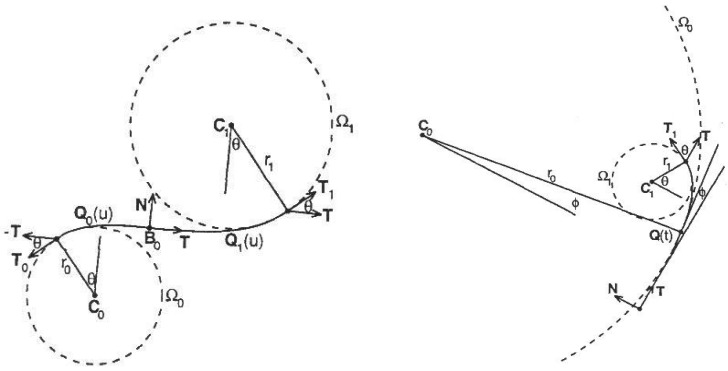

Figure 2: Third (left) and fifth (right) cases of circle to circle templates. (Baass, 1984; Walton and Meek, 1996; Meek and Walton, 1989).

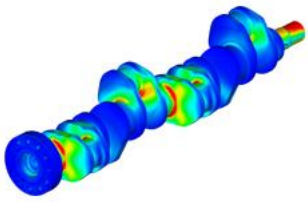

Figure 3: Automotive crankshaft in Linear Static Analysis.

2.0 NOMENCLATURE

Consider the notations such as symbol and unit in the nomenclature, as shown in Table 1. This nomenclature is the basic foundation of Linear Static Analysis (M Britto, 2005).

It is noticed that the unit of these input and output parameters will be based on the system of units that are applied in the solid model. Table 1 is extensively used for the analysis purposes. In the next section, we will explore the description method of the designing of spur gear using S transition and C spiral curves.

Table 1: Some of the parameters that are commonly used in the system of units

System of Units	Input Parameters				Output Parameters		
	Length, ζ	Force, f	Mass, η	Density, ρ	Displacement, δ	Force, f	Stress, υ
1	m	N	kg	kgm^{-3}	m	N	Pa
2	mm	N	mg	$mgmm^{-3}$	mm	N	MPa
3	ft	lb_f	slug	$slugft^{-3}$	ft	lb_f	psf
4	in	lb_f	$lb_f.s^2in^{-1}$	$lb_f.s^2in^{-4}$	in	lb_f	psi

3.0 METHOD OF DESCRIPTIONS

3.1 Bézier-Like Cubic Curve as a Function

Bézier-like cubic curve (also known as the cubic alternative curve) is a new basis function in the field of Computer Aided Geometric Design (CAGD). Bézier-like basis function simplifies the process of controlling the curve since it has only two shape parameters, λ_0 and λ_1 to control or change the shape of the curve such in Figure 4, compared to the cubic Bézier curve for which the control points need to be adjusted (Farin, 1997). Bézier-like cubic curve is formulated by applying the form of Hermite interpolation given by (Ali, 1994; Ali *et al.*, 1996; Ahmad, 2009).

$$z(t) = \varphi_0(t)P_0 + \varphi_1(t)P_1 + \varphi_2(t)P_2 + \varphi_3(t)P_3, \qquad 0 \le t \le 1 \tag{1}$$

with,

$$\begin{aligned} &\varphi_0(t) = (1-t)^2(1+(2-\lambda_0)t),\ \varphi_1(t) = \lambda_0(1-t)^2 t \\ &\varphi_2(t) = \lambda_1(1-t)t^2,\ \varphi_3(t) = t^2(1+(2-\lambda_1)(1-t)) \end{aligned} \tag{2}$$

where P_0, P_1, P_2, P_3 are the control points, and $\varphi_0(t), \varphi_1(t), \varphi_2(t), \varphi_3(t)$ are Bézier-like cubic basis functions. Hence, Bézier-like cubic curve can be written as

$$z(t) = (1-t)^2(1+(2-\lambda_0)t)P_0 + \lambda_0(1-t)^2 tP_1 + \lambda_1(1-t)t^2P_2 + t^2(1+(2-\lambda_1)(1-t))P_3 \tag{3}$$

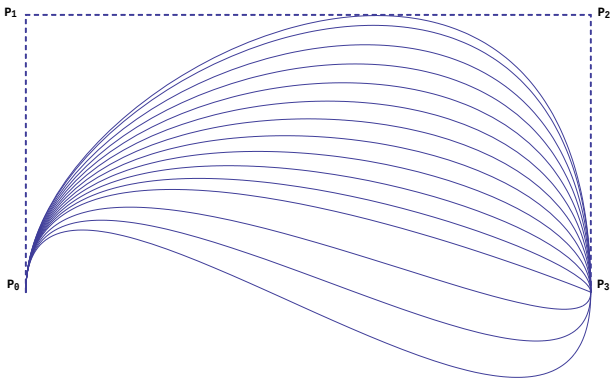

Figure 4: Distribution of Bézier-like cubic curves with the different values of λ_0 and λ_1.

In the next subsection, we will explain the control points identification in Bézier-like cubic curve based on the circle to circle template (Figure 2)

3.2 Third Case of Circle Templates as an S-Shaped Transition Curve

The cubic Bézier curve had been predominantly used in curve design, as shown in studies by Habib and Sakai (2003) and Walton and Meek (1999). The similarity between this function and Bézier-like cubic curve is that both functions have four control points. By referring to Habib and Sakai (2003), the control points are stated as

$$P_0 = c_0 + r_0 * \{\cos\alpha, \sin\alpha\}, \quad P_1 = P_0 + h * \{-\sin\alpha, \cos\alpha\}$$
$$P_3 = c_1 - r_1 * \{\cos\alpha, \sin\alpha\}, \quad P_2 = P_3 - k * \{-\sin\alpha, \cos\alpha\} \tag{4}$$

where, c_0 and c_1 are the centre points of circles ψ_0 and ψ_1, r_0 and r_1 are the radii of circles ψ_0 and ψ_1, h and k are the length or norm of $\|P_1, P_0\|$ and $\|P_3, P_2\|$ while α is an angle's circles measured anticlockwise. These control points are unique only in the case of the S-shaped transition curve. The improvements are made in Eq. (4) to increase the degree of freedom and its applicability such

$$P_0 = c_0 - r_0 * \{\cos\alpha, \sin\alpha\}, \quad P_1 = P_0 - h * \{-\sin\alpha, \cos\alpha\}$$
$$P_3 = c_1 + r_1 * \{\cos\beta, \sin\beta\}, \quad P_2 = P_3 + k * \{-\sin\beta, \cos\beta\} \tag{5}$$

with the angles in the circle $\{\psi_0, \psi_1\}$ denoted as α and β which are measured anticlockwise. The other parameters remain the same as in Eq. (4). The value of h and k will be calculated by using the curvature continuity (G^2 continuity) shown as

$$\kappa(t=0) = -\frac{1}{r_0}, \ \kappa(t=1) = \frac{1}{r_1} \tag{6}$$

By applying these theories, an S-shaped curve is demonstrated in Figure 5.

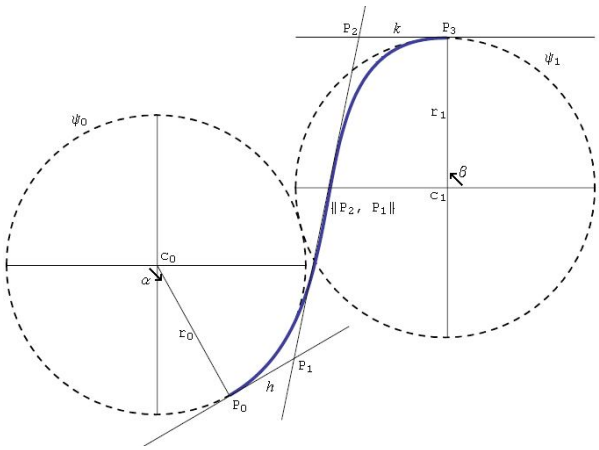

Figure 5: An S-shaped transition curve produced by using G^2 Bézier-like cubic curve.

3.3 Fifth Case of Circle Templates as a C-Shaped Spiral Curve

The fifth case will produce a type of C-shaped transition curve as a single spiral (Baass, 1984; Walton and Meek, 1996; Habib and Sakai, 2005). The curve architecture in transition and spiral curves is totally different from the segmentations used. As shown in Figure 6, three segments are needed to design C-shaped transition curve whereas only two segments are used in C-shaped spiral curve.

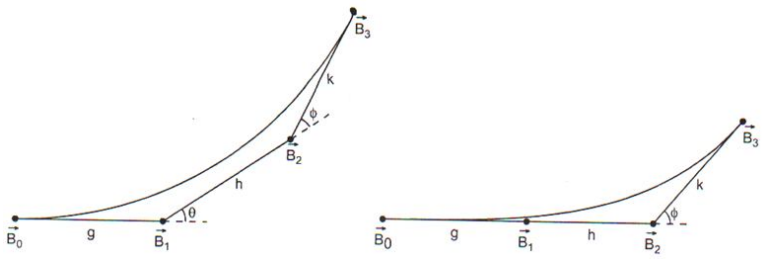

Figure 6: Transition (left) and spiral (right) curves architecture applied in cubic Bézier curve (Walton *et al.*, 2003).

We now identify the control points as in (Habib and Sakai, 2003)

$$P_0 = c_0 + r_0 * \{\cos\alpha, \sin\alpha\}, \quad P_1 = P_0 + h * \{-\sin\alpha, \cos\alpha\}$$
$$P_3 = c_1 - r_1 * \{\cos\beta, -\sin\beta\}, \quad P_2 = P_3 + k * \{\sin\beta, \cos\beta\} \tag{7}$$

Where the notations are the same as in Eq. (4). The definitions in Eq. (7) will produce a C-shaped transition curve which is related to the second case (Walton and Meek, 1999; Baass, 1984 ; Walton and Meek, 1996). Modifications of Eq. (7) are needed for fifth case template, and therefore, we have

$$P_0 = c_0 - r_0 * \{\cos\beta, \sin\beta\}, \quad P_1 = P_0 + k * \{\sin\beta, -\cos\beta\}$$
$$P_3 = c_1 + r_1 * \{\cos\alpha, \sin\alpha\}, \quad P_2 = P_3 - h * \{-\sin\alpha, \cos\alpha\} \tag{8}$$

where $\{c_0, r_0, \beta\}$ is the centre point, radii and angle of the circle, ψ_0 while the centre point, radii and angle in the circle, ψ_1 represented as $\{c_1, r_1, \alpha\}$. Parameter *h* and *k* are the length or norm of $\|P_3, P_2\|$ and $\|P_1, P_0\|$. In order to design C spiral curve, the segments used in Eq. (8) should be reduced (Walton *et al.*, 2003) by assuming that

$$P_1 = P_2 \tag{9}$$

Then, in Eq. (9) either *h* or *k* can be eliminated by using a dot product. If the parameter chosen is *k*, the expression will be dotted with a vector, $\{\cos\alpha, \sin\alpha\}$ where

$$k = \frac{((c_1 - c_0) \cdot \{\cos\alpha, \sin\alpha\}) + r_1 + r_0 * \cos[\alpha - \beta]}{\sin[\beta - \alpha]} \tag{10}$$

The modified control points that satisfy the fifth case template (C spiral curve) are given by

$$P_0 = c_0 - r_0 * \{\cos\beta, \sin\beta\}$$
$$P_1 = P_0 + k * \{\sin\beta, -\cos\beta\} \tag{11}$$
$$P_3 = c_1 + r_1 * \{\cos\alpha, \sin\alpha\}$$

In order to join C spiral curve with the circles, we will need to apply the curvature continuity such

$$\kappa(t=0) = \frac{1}{r_0}, \quad \kappa(t=1) = \frac{1}{r_1} \tag{12}$$

This continuity is also used to determine the shape parameters, λ_0 and λ_1 in Eq. (3). A generated C-shaped spiral curve is visualized in Figure 7.

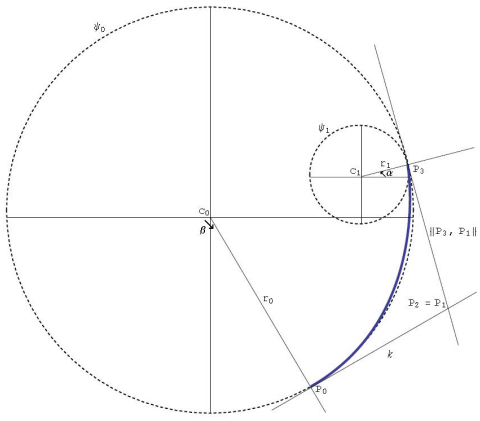

Figure 7: C-shaped curve in the fifth case of circle templates using G^2 Bézier-like cubic curve.

Both curve theories will be applied to redesign a profile (tooth) of the spur gear. Currently, an involute or evolute curve is always used in designing this spur tooth profile.

4.0 SPUR GEAR DESIGN

4.1 Modeling of Spur Gear

Traditional spur gears have the teeth which are straight and parallel to the axis of the shaft that conveys the gear (Mott, 2003). Normally, the teeth have an involute form where this form can be acted as in contacting the teeth (Mott, 2003). Figure 8 shows a schematic and related terminology for spur gear

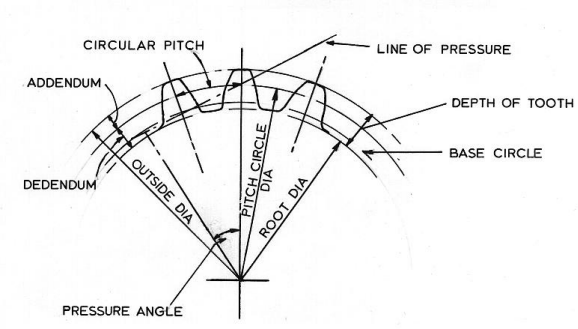

Figure 8: Some of the terms in spur gear (Price, 1995).

Based on Figure 8, an inner circle and an outer circle can be drawn, and smaller circles can be fitted within their boundaries, as shown in Figure 9. This resulting structure will be used to design a profile (tooth) of the spur gear.

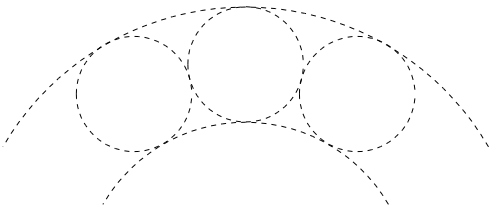

Figure 9: A new basis model of designing a spur gear tooth.

4.2 Single Tooth Design uses an S-Shaped Transition Curve

By applying the segmentation of divisions, two segments are divided to create this single tooth. This is because an S-shaped curve has the beginning point at the tangent of base circle and ending at the tangent of the outside circle. For the first segment, the inputs are c_0 = {-0.398, 0.689}, c_1 = {0, 0.795}, $\alpha = 0.6667\pi$ radian, $\beta = 0.5\pi$ radian, $r_0 = r_1 = 0.206$ are used, while for segment two, the inputs are c_0 = {0.398, 0.689}, c_1 = {0, 0.795}, $\alpha = 0.3333\pi$ radian, $\beta = 0.5\pi$ radian and other parameters remain the same as in segment one. Then, h and k are determined to be 0.2779 and 0.3780 in accordance with the inputs and theories above. Notice that, the value of h and k is similar in both segments. Figure 10 shows the design of the tooth and its segmentation using an S-shaped transition curve.

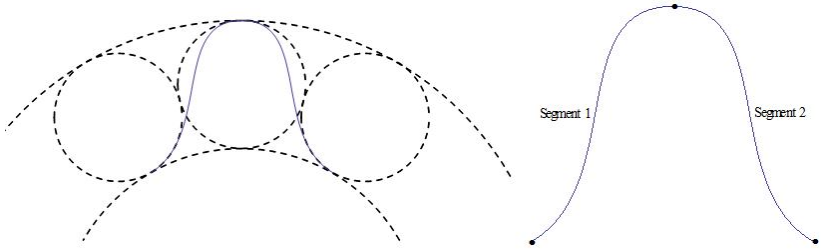

Figure 10: Single tooth of spur gear using an S-shaped transition curve (left) and its segmentation (right).

4.3 Single Tooth Design uses a C-Shaped Spiral Curve

In this case, Figure 9 is modified to suit the elements in designing a C-shaped spiral curve (Subsection 3.3). The small circles are drawn at the intersection of two circles. For this curve, it needs four segments to design a single tooth of the spur gear. Segment one consists of c_0 = {-0.398, 0.689}, c_1 = {-0.247, 0.725}, $\alpha = 0.05556\pi$ radian, $\beta = 0.6667\pi$ radian, $r_0 = 0.206$ and $r_1 = 0.05$. The values of k and shape parameters, λ_0, λ_1 are computed by using the Eqs. (3), (10), (11), and (12). We found that $k = 0.1431$ whereas λ_0 and λ_1 are equal to 2.7695 and 0.3619, respectively. For segment two, the inputs are c_0 = {0, 0.795}, c_1 = {-0.247, 0.725}, $\beta = 1.5\pi$ radian while the rest is exactly the same as in segment one. This time, k and shape parameters, λ_0, λ_1 are found to be 0.2449, 2.1279 and 0.5343, respectively. These two segments have a

symmetrical curve which can be defined as mirroring or balancing to segment three and four. Thus, segment three and four have the similar shape to segment one and two, respectively (Du Sautoy, 2009). Figure 11 shows the design of the tooth and its segmentation using this C spiral curve. Next, we will apply the single tooth designs using both developed curves in order to design a solid model of the spur gear.

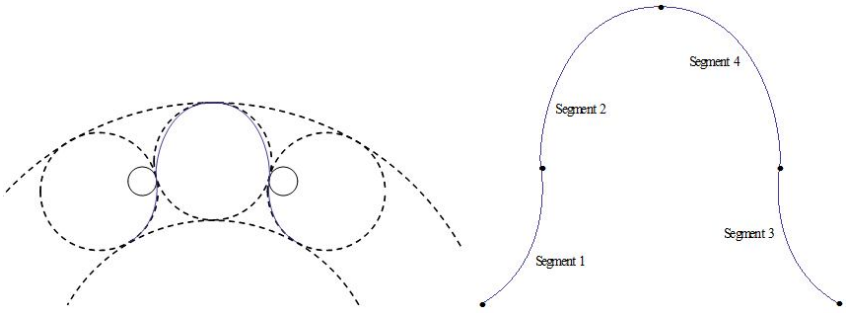

Figure 11: Single tooth of spur gear using a C-shaped spiral curve (left) and its segmentation (right).

4.4 S Transition and C Spiral as the Shaped Curves in Solid of Spur Gear

In Computer Aided Geometric Design (CAGD), the surface design technique is commonly used where this technique has several design and surface properties to be considered (Bloor *et al.*, 1995), difficult to extrude as a solid model and unsuitable in Computer Aided Analysis (CAE) purposes. To solve these problems, the integration of Mathematical and Computer-Aided Design (CAD) may be applied. Wolfram Mathematica 7.0 and CATIA V5 are both selected as the integrated software of the designing of the solid model of the spur gear. The following process flow diagram is used to show the integration of both software and its applications in spur gear design (Figure 12). Two models of six gear teeth are developed with the outside and shaft diameters as well as the gear thickness are 40.04 mm, 5.672 mm and 4 mm (Figure 13).

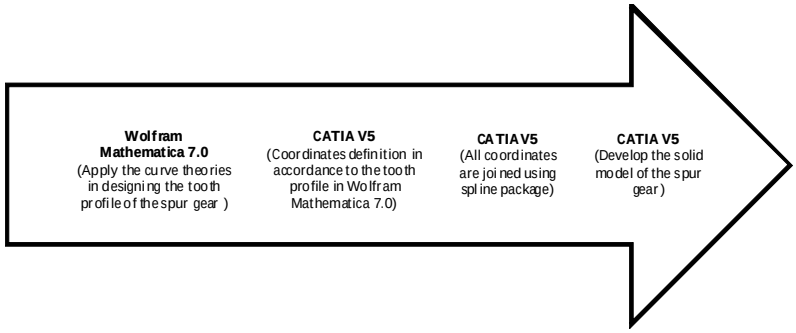

Figure 12: Integrated process flow diagram used in designing a solid model of the spur gear.

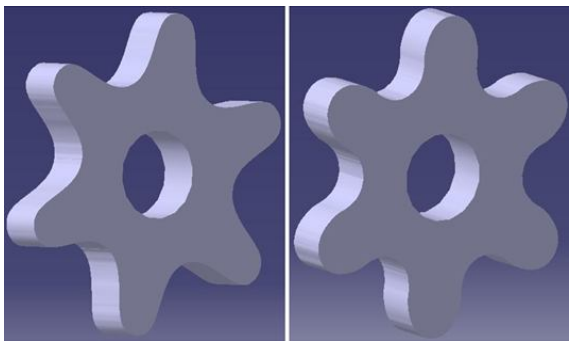

Figure 13: Solid of spur gear using S transition (left) and C spiral (right) curves.

We will extend these solid design structures to analyze its applicability of the new tooth profiles with the gear material using Linear Static Analysis.

5.0 LINEAR STATIC ANALYSIS

5.1 Fundamental of Linear Static Analysis

Most of the structural problems can be treated as a linear static problem if and only if the several

assumptions are made such as linear behavior, elastic material and static loads (Ziaei Rad, 2011). The scenario of the assumptions is shown in Figure 14. One of the applicabilities of Linear Static Analysis is to find out the structural response of the bodies' spinning with the effect of the velocities or accelerations are constants since the applied loads are static (do not change with time). This analysis measures the responses of the displacement, strain (deformation), stress and reaction force. The linear static problem can be simplified using the expression of the linear matrix system such

$$[K]\{x\} = \{F\} \tag{13}$$

where,

[*K*] is the structural (assembled) stiffness matrix or square matrix of order (*n x n*), {*x*} are the unknown parameters (displacement, strain and stress) of order (*n x* 1) while {*F*} is the loading in the system represents the matrix of the order (*n x* 1). For the solution of {*x*}, the matrix solver that will be used is FEA. The next subsection will explain the FEA solver and its structural modeling.

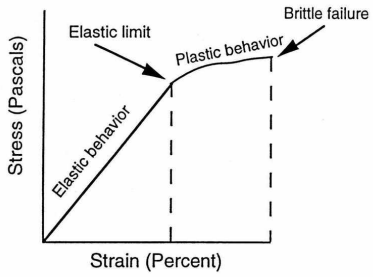

Figure 14: Linearity and elastic material assumptions in the static analysis (Hamburger, 2000).

5.2 FEA Solver and Its Modeling

MSC Nastran & Patran is the FEA software chosen as the preferred solution for Linear Static Analysis. The following process flow diagram is the FEA processes that will be applied using this software, as shown in Figure 15 (Sapto and Safarudin, 2008; Daryl, 2006).

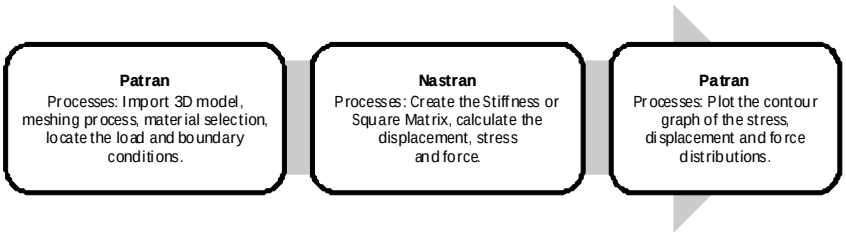

Figure 15: Process flow diagram of MSC Nastran & Patran and its FEA application.

5.2.1 CAD models and its meshes

The CAD or solid models (Figure 13) will be imported to MSC Patran software as the starting process of the Linear Static Analysis (FEA). The selection of the element model in FEA is very crucial and will be determined the overall process of the analysis. The gear structures (Figure 13) are the Three-Dimensional (3D) geometry solid models that reveal the complex structures. Solid element models are widely used to analyze the complex elements such as structural components and loading conditions and also the estimation of the stress levels (Fellipa, 2009; Entrekin, 1999). The element topology that is chosen for the structure (Figure 13) is Tetrahedral-10 (Tet-10) that represents a 3D solid triangle with four planar faces and ten nodes (Fellipa, 2009; Fellipa 2011), as shown in Figure 16. The Tet-10 or second order tetrahedral element is commonly used for its ability to mesh almost any solid regardless of its complexity (Entrekin, 1999; Said *et al.*, 2012). The resulting of the applied Tet-10 is shown in Table 2 and Figure 17.

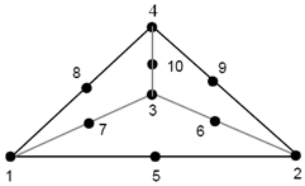

Figure 16: Tet-10 element's topology (Sapto and Safarudin, 2008; Fellipa, 2011).

Table 2: Tet-10 and its mesh data structures

Solid of the spur gear (S transition)			Solid of the spur gear (C spiral)		
Global Edge Length	Nodes	Elements	Global Edge Length	Nodes	Elements
1.0551234	34897	22448	1.011111	34854	22668

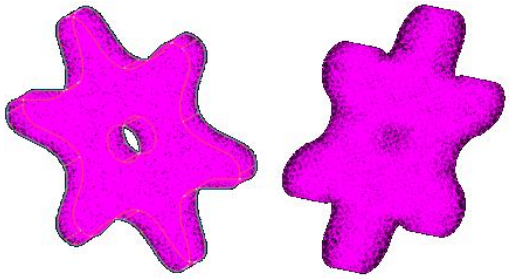

Figure 17: Tet-10 and its spur gear meshing of the applied curves, S transition (left) and C spiral (right).

5.2.2 Boundary and loading conditions

The next process is the setting of the boundary and loading conditions on the solid model (Figure 17). Boundary condition can be referred as the external load on the border of the structure (Feng, 2011). As this case, the boundary condition is applied on the gear shaft (Figure 17) where in this shaft, the displacement does not happen (is equivalent to zero) (Nikolić *et al.*, 2012; Lee, 2009). This is the important setting to simulate the gear transmission (Feng, 2011). Many of the references used Torque (*T*) as the applied load (loading condition) for their analysis and application (Feng, 2011; Nikolić *et al.*, 2012; Lee, 2009). In order to find out the new tooth profiles and its applicability (Figure 13), the suitable load to be applied is Pressure (*P*) which this load is set on the contact stress of both spur gear models (Figure 17) (Gilbert Gedeon, 1999; Wang *et al.*, 2011). The critical region of the contact stress is shown in Figure 18 (Rameshkumar *et al.*, 2010). Figure 19 shows the setting of both conditions in the models (Figure 17). One of the conditions, *P* is applied as 50 MPa

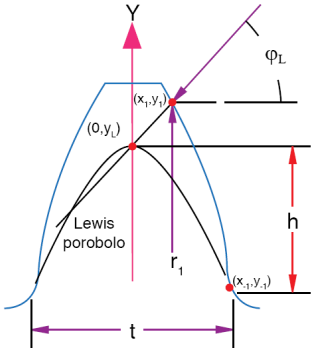

Figure 18: The critical region (two dots along the blue line) of the contact stress in the tooth profile (Rameshkumar *et al.*, 2010).

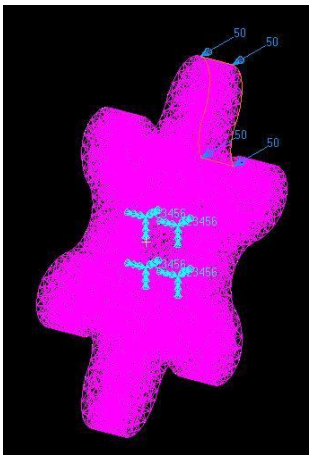

Figure 19: Spur gear model using C-spiral curve with its boundary conditions and load, *P* = 50 MPa.

5.2.3 Material selection for spur gear

Stainless Steel Grade 304 also known as AISI 304 is widely used in the range of applications such as a gear material (Zehe *et al.*, 2002). This grade of material is the type of Austenitic Stainless Steels for the highly contained of Chromium and Nickel. These Steels have high ductility and ultimate tensile strength and also low yield stress. Figure 20 shows one of the cases of Austenitic Stainless Steels when compare to a Typical Carbon Steel. It can be seen clearly that the stability region is occurred in the types of Austenitic while the Carbon type has an instability diagram (Figure 20). The mechanical properties of the AISI 304 are presented in Table 3. These properties will be used in this static analysis.

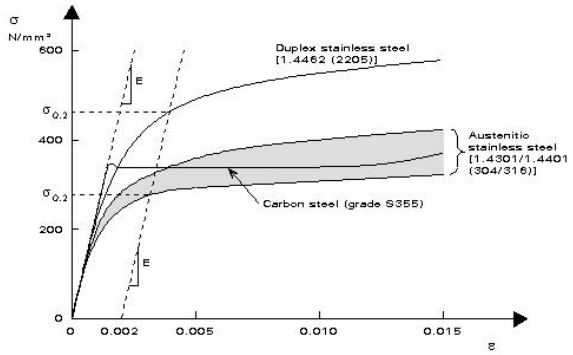

Figure 20: Stress-strain behavior of the Austenitic and Carbon Steels.

After applying the above settings on the models (Figure 19), it is ready to analyze using MSC Nastran & Patran software (Figure 15). The processor of Intel ® Core ™ 2 Duo CPU with the RAM, 3.49 GB is used to operate the software. The resulting of this process will be discussed in the next subsection.

Table 3: AISI 304 and its characteristics (Peckner and Bernstein, 1977)

Modulus of Elasticity	Yield Strength	Ultimate Strength	Poisson Ratio	Density	Damping Coefficient
195 GPa	215 MPa	505 MPa	0.29	8 gcc^{-1}	0.003

5.2.4 Simulation results and its safety factor

The discussion began with the presentation of the generated results using Linear Static Analysis. These results of the proposed models will be compared with the existing model. The existing model (EM) is directly designed using the graphical properties in CATIA V5 with the dimensions remained the same. Table 4 shows the maximum Von Mises stress (υ_{max}) and maximum displacement (δ_{max}) distributions among the models through the repeated loads. Hence, the safety factor (S_f) or also known as a design margin (Michalopoulos and Babka, 2000) can be derived as in Eq. (14) (Clifford *et al.*, 2008; Shenoy, 2004) and where the yield strength of AISI 304 can be found in Table 3.

$$S_f = \frac{Yield\ Strength\ of\ \ AISI\ 304}{\upsilon_{max}} \tag{14}$$

Table 4: The result distributions of δ_{max}, υ_{max} and S_f in the applied models

P (MPa)	EM			S Transition			C Spiral		
	δ_{max} (mm)	υ_{max} (MPa)	S_f	δ_{max} (mm)	υ_{max} (MPa)	S_f	δ_{max} (mm)	υ_{max} (MPa)	S_f
10	5.93E-3	61.3	3.507	5.99E-3	61.9	3.473	5.77E-3	62.5	3.440
20	1.19E-2	123	1.748	1.20E-2	124	1.734	1.15E-2	125	1.720
30	1.78E-2	184	1.168	1.80E-2	186	1.156	1.73E-2	187	1.150
40	2.37E-2	245	0.878	2.40E-2	248	0.867	2.31E-2	250	0.860
50	2.97E-2	307	0.700	3.00E-2	309	0.696	2.89E-2	312	0.689

Figure 21 depicts the contour plot of determining the presented values of υ_{max} and δ_{max} (Table 4) for the applied *P* = 30 MPa. It is clearly shown in the plot legend that δ_{max} approximates to 1.73E-2 at the node, 34450 while the value of υ_{max} is equal to 187 MPa at the node, 27631. The υ_{max}

(red color) occurs in the gear shaft because of the model (Figure 17) is analyzed in the steady state (static) behavior (Boulos *et al.,* 1997). The resulting of υ_{max} (P = 30 MPa) is far below the yield strength of AISI 304. Therefore, S_f approximates to 1.15 (Table 4). Failure occurs if and only if $S_f < 1$ or S_f has the negative sign (Michalopoulos and Babka, 2000). All gear models in Table 4 are safe to be used if $P \leq 30$ MPa whereas the models are in failure modes if $P > 30$ MPa. These inequalities show that the new teeth profiles (S transition and C spiral curves) have the same applicability (strength) when compare to the EM. The findings in Table 4 will be used to predict when the failure (fatigue) modes start to occur among the gear models. This fatigue prediction will be discussed in the next section.

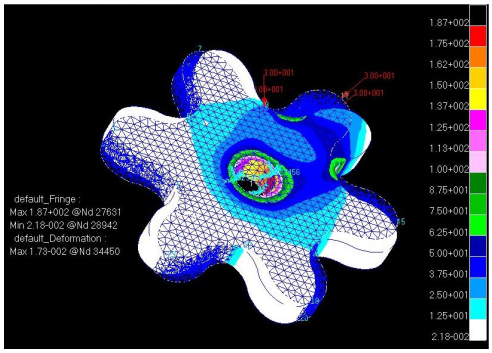

Figure 21: The example of findings $\{\delta_{max}, \upsilon_{max}\}$ for the applied P = 30 MPa in C spiral gear model.

6.0 FIRST-ORDER NEWTON INTERPOLATING POLYNOMIAL AS A FATIGUE PREDICTOR

Fatigue can be described as a failure mode that happened on the structure design which this structure is affected by the implications of repeated or varying loads, fluctuating loads and rapidly applied loads (Pun, 2001). Fatigue also can be occurred by the different physical mechanisms such as low-cycle and high-cycle fatigue (Pun, 2001). As referred to in failure mode above, let assume that the fatigue starts to occur if $S_f = 1$. Due to this S_f, the related load will be predicted using the Newton's Interpolating Polynomial. The general form of this polynomial such (Chapra and Canale, 2010).

$$f_n(x) = b_0 + b_1(x - x_0) + b_2(x - x_0)(x - x_1) + \ldots + b_n(x - x_0)(x - x_1)\ldots(x - x_{n-1}) \tag{15}$$

Where, n is referred to as the nth-order polynomial, b_0, b_1, b_2 and b_n are the polynomial coefficients and the set of (n+1) data points represented by $\{x_i, f(x_i)\}$ with $i = \{0, 1, 2, 3, \ldots, n\}$. The polynomial coefficients also can be shown as (Chapra and Canale, 2010).

$$b_0 = f(x_0); b_1 = f[x_1, x_0]; b_2 = f[x_2, x_1, x_0]; b_n = f[x_n, x_{n-1}, \ldots, x_1, x_0] \tag{16}$$

And the bracketed functions are evaluated using the Finite Divided Differences where (Chapra and Canale, 2010).

$$f[x_1, x_0] = \frac{f(x_1) - f(x_0)}{x_1 - x_0}; \; f[x_2, x_1, x_0] = \frac{f[x_2, x_1] - f[x_1, x_0]}{x_2 - x_0};$$
$$f[x_n, x_{n-1}, \ldots, x_1, x_0] = \frac{f[x_n, x_{n-1}, \ldots, x_1] - f[x_{n-1}, x_{n-2}, \ldots, x_0]}{x_n - x_0} \tag{17}$$

We can see clearly in Table 4 that the fatigue of the models starts to occur in the range of $P \in [30, 40]$ that allows only two data points. Therefore, the First-Order Newton Interpolating Polynomial or known as Linear Interpolation is the suitable polynomial to be applied. Let P is denoted as x-axis while S_f is equal to $f(x)$ or y-axis. The first-order or linear form (n = 1) is given as

$$f_1(x) = b_0 + b_1(x - x_0) \tag{18}$$

With b_0 and b_1 are calculated using Eqs. (16) and (17). The algorithms of using this linear interpolation include four steps such as: Set x_0, x_1, $f(x_0)$ and $f(x_1)$; Calculate b_0 and b_1; Substitute x_0, b_0 and b_1 into $f_1(x)$; Solve x

for $f_1(x) = 1$. All calculated values of x among the models (Table 4) are fully depicted in Table 5. It shows that the models are in safety mode if $P \leq 35$ MPa while the fatigue may start occurring when $P > 35$ MPa.

Table 5: The Initial loads of P for the fatigue mode

EM	S Transition	C Spiral
35.7931 MPa	35.3979 MPa	35.1724 MPa

With the reference of Table 5, the values in this table will be used to determine the Design Efficiency (DE) for the proposed models. Further discussion of DE will be explained in the following section.

7.0 DESIGN EFFICIENCY OF THE PROPOSED DESIGN MODELS

Design Efficiency (DE) or Sensitivity Analysis (SA) relates to the design quality (Aas, 2000; Azarian *et al.*, 2011) that can achieve the stated objectives of the certain studies such in this study, to find out the applicability of the new teeth design with AISI 304 as the selected material. Generally, the levels of DE in the engineering field are almost 85 % and above. Hence, 85 % can be assumed as the benchmark of the improvements that will be made (Gupta *et al.*, 2006). Let make the assumptions in Table 5 that EM equivalents to the true value, x_t (input) whereas S Transition and C Spiral are represented as the approximation values, x_a (output). Thus, DE can be expressed as (Khai *et al.*, 2007).

$$DE = \left(\frac{Output}{Input} = \frac{x_a}{x_t}\right) \times 100\% \tag{19}$$

After applying Eq. (19), DE of an S Transition approaches to 99% while for C Spiral method approximates to 98%. Both results have shown that DE almost achieved 100% of the design effectiveness. With reference to the above mentioned benchmark (85%), the proposed designs are the acceptable methods of designing the spur gear teeth with AISI 304 as the selected material.

8.0 CONCLUSIONS AND FUTURE WORK

This study has proposed the designing of spur gear teeth using S-shaped transition and C-shaped spiral curves (directly produced). Circle to circle templates have successfully been applied in both curves design. The solids of spur gear have been generated by the integration between Mathematical and CAD software. The applicability of the proposed design and the material, AISI 304 is measured using Linear Static Analysis, Fatigue Analysis and DE. First-order Newton interpolating polynomial can be employed as a fatigue predictor for all design models. As referred to in Table 4, all models are in safety mode if $P \leq 30$ MPa while in failure mode if $P > 30$ MPa. Generally, fatigue starts to occur when $P > 35$ MPa in all design models whereas the models are safe to use in the related applications if $P \leq 35$ MPa. The applicability (strength) of the proposed design, S and C curves are the same when compare to EM as shown in the above analyses. The new design methods, S and C curves are the acceptable methods of designing the spur gear teeth as both methods have presented DE greater than 85 % of the design effectiveness. In future, this study will continue in the analysis of dynamic and acoustic features such as normal, frequency and transient modes and also in the noise test.

ACKNOWLEDMENT

This research was supported by Universiti Teknikal Malaysia Melaka under the Fundamental Research Grant Scheme (FRGS). The authors gratefully acknowledge everyone who contributed helpful suggestions comments.

REFERENCES

[1] Ali, J.M. (1994): An Alternative Derivation of Said Basic Function. *Journal of Sains Malaysiana,* Vol.23, No.3, pp. 42-56.

[2] Ali, J.M., Said, H.B. and Majid, A.A. (1996): Shape Control of Parametric Cubic Curves. *SPIE, Fourth International Conference on Computer-Aided Design and Computer Graphics,* Zhou, J. (Ed), Vol.2644, pp.128-133.

[3] Ahmad, A. (2009): Parametric Spiral and its Application as Transition Curve. *Ph.D Thesis*, Universiti Sains Malaysia, pp.19-22.

[4] Aas, E.J. (2000): Design Quality and Design Efficiency; Definitions, Metrics and Relevant Design Experiences. *International Symposium on Quality of Electronic Design*, 20-22 March, San Jose, CA, USA.

[5] Azarian, A., Vasseur, O., Bennaï, B., Jolivet, V., Claeys-Bruno, M., Sergent, M. and Bourdon, P. (2011): Sensitivity Analysis of Interference Optical Systems by Numerical Designs. *Journal de la Société Française de Statistique*, Vol.152, No.1, pp.118-130.
[6] Babu, V.S. and Tsegaw, A.A. (2009): Involute Spur Gear Template Development by Parametric Technique using Computer Aided Design. *African Research Review,* Vol.3, No.1, pp. 1-6.
[7] Bradford, L.J. and Guillet, G.L. (1943), *Kinematics and Machine Design,* John Wiley & Sons, New York.
[8] Baass, K.G. (1984): The Use of Clothoid Templates in Highway Design. *Transportation Forum,* Vol.1, pp.47-52.
[9] Bloor, M.I.G., Wilson, M.J. and Hagen, H. (1995): The Smoothing Properties of Variational Schemes for Surface Design. *Computer Aided Geometric Design,* pp.381-394.
[10] Boulos, P.F., Wood, D.J. and Lingireddy, S. (1997): Pressure Vessels and Piping Systems-Shock and Water Hammer Loading. *Encyclopaedia of Life Support Systems (EOLSS)*, American Water Works Association, UNESCO.
[11] Clifford, K.H., Bibeau, T.A. and Quinones, A.Sr. (2008): Finite Element Analyses of Continuous Filament Ties for Masonry Applications: Final Report for the Arquin Corporation. *SAND2006-3750*, Sandia National Laboratories Albuquerque, California, USA.
[12] Chapra, S.C. and Canale, R.P. (2010): *Numerical Methods for Engineers, 6th Edn*. McGraw-Hill, New York.
[13] Du Sautoy, M. (2009): *Symmetry: A Journey into the Patterns of Nature,* HarperCollins, UK.
[14] Daryl, L. (2006): *A First Course in Finite Element Analysis,* Brookscole, Singapore.
[15] Entrekin, A. (1999): Accuracy of MSC/Nastran First and Second Order Tetrahedral Elements in Solid Modeling for Stress Analysis. *MSC Aerospace Users' Conference Proceedings*.
[16] Farin, G. (1997): *Curves and Surfaces for Computer Aided Geometric Design*, *A Practical Guide, 4th Edition,* Academic Press, New York.
[17] Fellipa, C. (2009): Solid Element: Overview. *Advanced Finite Element Method for Solid, Plates and Shells (ASEN 6367)*, 5 March, University of Colorado, Boulder, USA.
[18] Fellipa, C. (2011): The Quadratic Tetrahedron. *Advanced Finite Element Method for Solid, Plates and Shells (ASEN 6367)*, 7 May, University of Colorado, Boulder, USA.
[19] Feng, X. (2011): Analysis of Field of Stress and Displacement in Process of Meshing Gears. *International Journal of Digital Content Technology and its Applications*, Vol.5, No.6, pp.345-357.
[20] Firth, A. and Long, H. (2010): A Design Software Tool for Conceptual Design of Wind Turbine Gearboxes. *Europe's Premier Wind Energy Event*, 20-23 April, Warsaw, Poland.
[21] Gilbert Gedeon, P.E. (1999): Gears in Lubrication of Gears and Bearings. *EM 1110-2-1424*, 28 February, Stony Point, New York.
[22] Gupta, S., Tewari, P.C. and Sharma, A.K. (2006): TPM Concept and Implementation Approach. *Maintenance World*, 21 August, pp.1-18.
[23] Gurumani, R. and Shanmugam, S. (2011): Modeling and Contact Analysis of Crowned Spur Gear Teeth. *Engineering Mechanics*, Vol.18, No.1, pp.65-78.
[24] Habib, Z. and Sakai, M. (2003): G^2 Planar Cubic Transition between Two Circles. *International Journal of Computer Mathematics,* Vol.8, pp.959-967.
[25] Habib, Z. and Sakai, M. (2005): Circle to Circle Transition with a Single Cubic Spiral. *The Fifth IASTED International Conference Visualization, Imaging and Image Processing*, 7-9 September, Benidorm, Spain, pp. 691-696.
[26] Habib, Z. and Sakai, M. (2008): G^2 Cubic Transition between Two Circles with Shape Control. *Journal of Computational and Applied Mathematics*, Vol.223, pp.133-144.
[27] Hamburger, M. (2000): Stress, Strain and the Physics of Earthquake Generation. *G141 Earthquakes and Volcanoes*, 25 October, Indiana University, USA.
[28] Higuchi, F. and Gofuku, S. (2007): Approximation of Involute Curves for CAD-System Processing. *Engineering with Computers*, Vol.23, pp.207-214.
[29] Khai, N.M., Ha, P.Q. and Oborn, I. (2007): Nutrient Flows in Small-Scale Peri-Urban Vegetable Farming Systems in Southeast Asia-A Case Study in Hanoi. *Agriculture, Ecosystems and Environment*, Vol.122, No.2, pp.192-202.
[30] Lee, C.H. (2009): Non Linear Analysis of Spur Gear using Matlab Code. *M.Sc. Thesis*, California Polytechnic State University.
[31] Margalit, D. (1995): *History of Curvature*. *Concept of Curvature*, Brown University, USA.
[32] M Britto, A. (2005): Patran Beginner's Guide. *Department of Engineering*, 15 April, University of Cambridge, UK.
[33] Meek, D.S. and Walton, D.J. (1989): The Use of Cornu Spirals in Drawing Planar Curves of Controlled Curvature. *Journal of Computational and Applied Mathematics*, Vol.25, pp.69-78.
[34] Michalopoulos, E. and Babka, S. (2000): Evaluation of Pipeline Design Factors. *GRI 00/0076*, The Hartford Steam Boiler Inspection and Insurance Company, Hartford, USA.
[35] Mott, R.L. (2003), *Machine Elements in Mechanical Design Fourth Edition*, Prentice Hall, New Jersey.

[36] Niederstucke, B., Anders, A., Dalhoff, P. and Grzybowski, R. (2003): Load Data Analysis for Wind Turbine Gearboxes. *Final Report of Enhanced Life Analysis of Wind Power Systems*, Hamburg, German.
[37] Nikolić, V., Dolićanin, Ć. and Dimitrijević, D. (2012): Dynamic Model for the Stress and Strain State Analysis of a Spur Gear Transmission. *Strojniški Vestnik-Journal of Mechanical Engineering*, Vol. 58, pp.56-67.
[38] Peckner, D. and Bernstein, I.M. (1977): *Handbook of Stainless Steels*, McGraw-Hill, New York.
[39] Price, D. (1995): Spur Gears. *Mechanical Engineering Design Topics,* 9 August, GlobalSpec.
[40] Pun, A. (2001): How to Predict Fatigue Life. *Design News*, 17 December, Lexington, USA.
[41] Rameshkumar, M., Sivakumar, P., Sudesh, S. and Gopinath, K. (2010): Load Sharing Analysis of High-Contact-Ratio Spur Gears in Military Tracked Vehicle Application. *Gear Technology*, pp.43-50.
[42] Rashid, A. and Habib, Z. (2010): Gear Tooth Designing with Cubic Bézier Transition Curve. *Graduate Colloquium on Computer Sciences (GCCS)*, Vol.2, No.1, 16 June, Lahore, Pakistan.
[43] Reagor, C.P. (2010): An Optimal Gear Design Method for Minimization of Transmission Error and Vibration Excitation. *Ph.D Thesis*, Pennsylvania State University, USA.
[44] Reyes, O., Rebolledo, A. and Sanchez, G. (2008): Algorithm to Describe the Ideal Spur Gear Profile. *The World Congress on Engineering, II*, 2-4 July, London, UK.
[45] Said, M.R., Yuhazri, M.Y. and Lau, S. (2012): The Finite Element Analysis on Hexagonal Ring under Simple Lateral Loading. *Global Engineers and Technologists Review*, Vol.2, No.2, pp.1-7.
[46] Sapto, W.W. and Safarudin, M. (2008): Finite Element Analysis of Wide Rim Alloy Wheel. *National Conference on Design and Concurrent Engineering,* 28-29 October, Melaka, Malaysia, pp.407-411.
[47] Shenoy, P.S. (2004): Dynamic Load Analysis and Optimization of Connecting Rod. *M.Sc. Thesis*, University of Toledo.
[48] Walton, D.J. and Meek, D.S. (1999): Planar G^2 Transition between Two Circles with Fair Cubic Bézier Curve. *Computer Aided Design,* Vol.31, pp.857-866.
[49] Walton, D.J. and Meek, D.S. (1996): A Planar Cubic Bézier Spiral. *Journal of Computational and Applied Mathematics,* Vol.72, pp.85-100.
[50] Walton, D.J., Meek, D.S. and Ali J.M. (2003): Planar G^2 Transition Curves Composed of Cubic Bézier Spiral Segments. *Journal of Computational and Applied Mathematics,* Vol.157, pp.453-476.
[51] Wang, P.Y., Fan, S.C. and Huang, Z.G. (2011): Spiral Bevel Gear Dynamic Contact and Tooth Impact Analysis. *Journal of Mechanical Design*, Vol.133, No.8, pp.084501-1-084501-6.
[52] Westland, A. (2006): *Aerospace Structural Analysis,* Jesmond Engineering Limited, East Yorkshire, UK.
[53] Yeung, K.S. (1999): Analysis of a New Concept in Spline Design for Transmission Output Shafts. *BEASY Publications*, Southampton, UK.
[54] Ziaei Rad, S. (2011): Bar Linear Static Analysis. *Finite Element Method,* Isfahan University of Technology, Iran.
[55] Zehe, M.J., Gordon, S. and McBride, B.J. (2002): CAP: Computer Code for Generating Tabular Thermodynamic Functions from NASA Lewis Coefficients. *NASA/TP–2001–210959/REV1*, Glenn Research Center, Ohio, USA.